Steady-state and dynamic validation of a parabolic through collector model using the ThermoCycle Modelica library

Adriano Desideri[a,*], Remi Dickes[a], Javier Bonilla[b], Loreto Valenzuela[b], Sylvain Quoilin[a], Vincent Lemort[a]

[a]*Thermodynamics laboratory, University of Liège, Campus du Sart Tilman, B49, B-4000 Liège, Belgium*
[b]*PSA-CIEMAT, Plataforma Solar de Almería - Centro de Investigaciones Energéticas, MedioAmbientales y Tecnolgicas, Crta. de Senés s/n, 04200, Tabernas (Almería), Spain*

Abstract

Keywords: Dynamic modelling, dynamic validation

1. Introduction

Recent studies have envisaged the potential of small-capacity ORC-based CSP plants in case the future distributed energy scenario is considered [1, 2]. These power systems have been studied and prototypes were constructed in the 70's [3, 4]. Among CSP technologies, parabolic trough collectors allow reaching temperatures that perfectly fit the working conditions of ORC systems. In order to investigate the transients related to ORC-based CSP plants, it is fundamental to consider the transient related to the solar field. Dynamic models of parabolic trough collectors date back from the late '70s. Ray [5] presented in 1980 a non-linear dynamic model of a parabolic trough unit for direct steam generation. The finite volume modelling approach was adopted and the transient response of the model under different step disturbances was presented as typical results. Hirisch et al. [6] presented a finite volume based solar collector model of a DSG plant and a preliminary validation based on the first experimental results of the DISS facility at the plataforma solar the Almeria. A recent work from [7] reported a clear review of the major MB heat exchanger models capable of handling two-phase flows, and presented a moving boundary library developed in the Modelica language for the modelling of direct steam generation parabolic trough solar collectors.
Overall there is a lack of systematic work covering the validation of dynamic models for small-scale ORC power systems.

2. Parabolic trough collector modelling

The parabolic trough model is developed in the Modelica language [8] and is part of the open-source ThermoCycle library [9]. As depicted in Figure 1a, the model relies on a finite-volume approach for the modelling of the heat

*Corresponding author
Email address: adesideri@ulg.ac.be (Adriano Desideri)

Nomenclature

Acronyms

WHR	Waste heat recovery
ORC	Organic Rankine cycle
PI	Proportional integer
APS	Absolute pressure sensor
RTD	Resistance temperature detector
CFM	Coriolis flow meter
UFM	Ultrasonic flow meter
DPS	Pressure difference transmitter
PLC	Programmable logic controller

Subscripts

P	pump
nom	nominal
n	reference
int	internal
ext	external
pred	predicted
meas	measured
su	supply
el	electrical
ex	exit
sf	secondary fluid
wf	working fluid
is	isentropic
w	wall
l	lateral
exp	expander

Symbols

p	pressure (bar)
T	temperature (°C)
s	entropy ($kJkg^{-1}K^{-1}$)
$\dot{V}$	volume flow rate ($m^3.s^{-1}$)
V_s	swept volume (m^3)
$\dot{q}$	heat flux ($kW.m^{-2}$)
M	mass (kg)
h	specific enthalpy ($kJ.kg^{-1}$)
ρ	density ($kg\ m^{-3}$)
A	area (m^2)
N	rotational speed (rpm)
Φ	filling factor
$\dot{W}$	electrical power (kW)
$\dot{m}$	mass flow ($kg.s^{-1}$)
U	heat transfer coefficient ($kJ.(kg.K)^{-1}$)
ε	efficiency

collection element (HCE), which is discretized along its axial axis in N constant and uniform control volumes (CV). The one-dimensional modelling method is justified by the large ratio between the diameter and the length of the HCE. Following the object-oriented formalism of Modelica, the PTC model is built by interconnecting two sub-components, i.e. the *Flow1D* and the *SolAbs* models. These two are linked together through a thermal port as depicted in Figure 1b.

The *Flow1D* component simulates the fluid flow in the HCE. In each CV, both mass and energy balances are solved assuming an incompressible fluid and a static momentum balance. Considering the above mentioned assumptions, the final conservation law formulations for each CV are reported in Equations 1 to 3, taking pressure, p, and specific

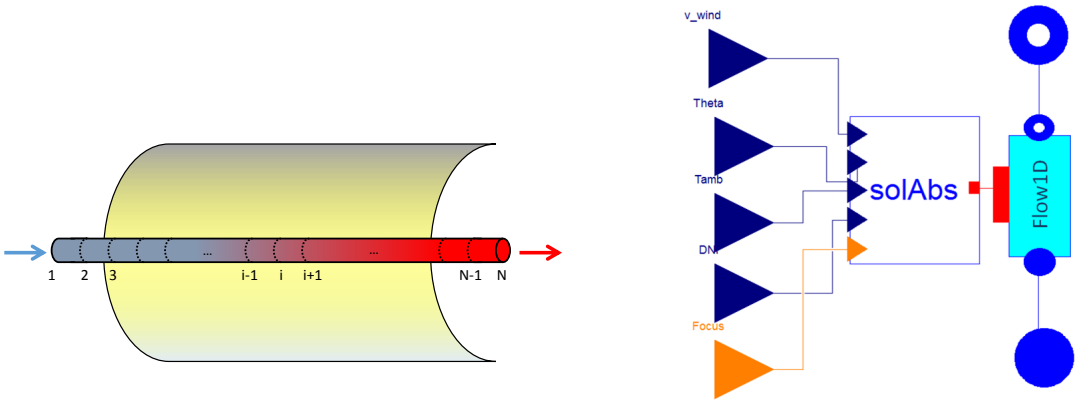

(a) (b)

Figure 1: Parabolic trough collector model in ThermoCycle. 1a: One-dimensional finite-volume modelling of the PTC. 1b: Object diagram of the solar collector model from the GUI of Dymola.

enthalpy, h, as dynamic state variables.

$$\frac{dM}{dt} = \dot{m}_{su} - \dot{m}_{ex} = 0 \quad \text{with} \quad \frac{dM}{dt} = V\left(\frac{\partial\rho}{\partial h}\cdot\frac{dh}{dt} + \frac{\partial\rho}{\partial p}\cdot\frac{dp}{dt}\right) \tag{1}$$

$$V\rho\frac{dh}{dt} = \dot{m}_{su}(h_{su} - h) - \dot{m}_{ex}(h_{ex} - h) + V\frac{dp}{dt} + A\cdot\dot{q}_{conv,fl} \tag{2}$$

$$p_{su} = p_{ex} \tag{3}$$

where $\partial\rho/\partial h$ and $\partial\rho/\partial p$ are thermodynamic properties of the fluid directly computed by the open-source CoolProp library [10]. The "su" (supply) and "ex" (exhaust) subscripts denote the nodes variable of each CV, A is the lateral surface through which the heat flux $\dot{q}_{conv,fl}$ is transferred to the fluid and V is the constant volume of each CV. An upwind discretization scheme is selected.

The *SolAbs* submodel simulates the effective thermal energy transferred from the ambient through the HCE to the fluid. The model is built upon Forristall steady-state equations [11] and implements the dynamic 1D radial energy balance around the HCE, see Figure 2. The model relies on physics-based equations and accounts for:

- conduction and thermal energy accumulation in the metal pipe;
- convection and radiation between the glass envelope and the metal pipe;
- conduction and thermal energy accumulation in the glass envelope;
- radiation and convection losses to the environment.

Such modelling approach allows simulating the relationship between the environmental parameters (DNI , Θ_{incid}, T_{amb}, v_{wind}) and the axial temperature distribution along the absorber tube. The thermal power transferred to the fluid

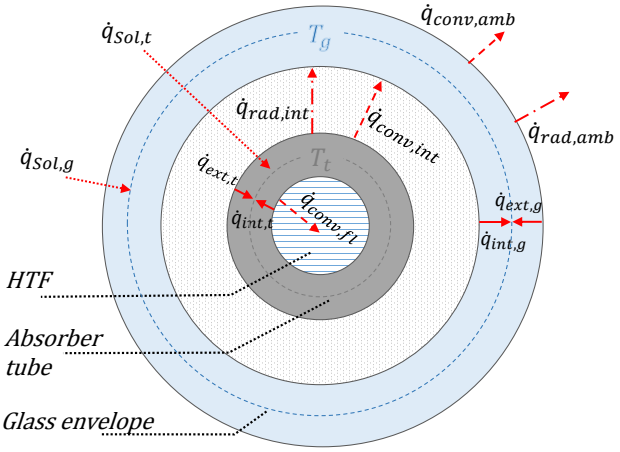

Figure 2: Energy balance around the HCE. In blue the glass envelope, in grey the metal pipe and in white the vacuum between the two. Heat transfer is highlighted with red arrows.

($\dot{q}_{conv,fl}$), the losses to the environment ($\dot{q}_{conv,amb} + \dot{q}_{rad,amb}$) and the temperatures of both the metal pipe (T_t) and the glass envelope (T_g) can then be evaluated. Temperatures, heat transfer coefficients and thermodynamic properties are considered uniform around the circumference of the HCE (1D model). Heat losses through the support brackets are neglected and solar absorptions in the tube and the glass envelope are treated as a linear phenomenon. Unlike Forristall's original model, the energy balance in the glass envelope and the metal pipe is calculated accounting for their thermal capacitance as shown in Equations 4-5.

$$\rho_g C_{p,g} \frac{dT_g}{dt} = \dot{q}_{int,g} D_{int,g} \pi + \dot{q}_{ext,g} D_{ext,g} \pi \tag{4}$$

$$\rho_t C_{p,t} \frac{dT_t}{dt} = \dot{q}_{int,t} D_{int,t} \pi + \dot{q}_{ext,t} D_{ext,t} \pi \tag{5}$$

For a detailed description of all the heat transfer equations between the different elements, please refer to [11] and [12].

3. Measurements and experiments

3.1. Experimental facility

An aerial view of the PTTL system is shown in Figure 3. The solar field was characterized by three parallel lines of parabolic trough collectors (PTC) from different manufacturers AlbiasaTrough, EuroTrough and UrssaTrough. The system was a closed loop, with an East-West orientation and it is charged with the thermal oil Syltherm 800 [13]. The process flow diagram of the PTTL facility is shown in Figure 4. Looking at the bottom of Figure 4 it is possible to recognize the pump which drove the fluid, in liquid state, through one of the three parallel PTC lines of the solar field. The fluid was heated from (2) to (3) by absorbing the solar energy reflected by the collectors to the receiver tubes. At the outlet of the collectors the fluid was cooled down by air-cooler II characterized by a maximum thermal capacity

Figure 3: Aerial view of the PTTL facility at PSA, Almería

of 400 kW_{th}. Once cooled down the oil reached the pump suction port (1). A 1 m^3 expansion vessel with Nitrogen, N_2, inertization placed in between the two air coolers was used to regulate the loop pressure which was limited to 18 bar. In the whole circuit the oil was maintained in liquid state. Two electric heaters installed at the outlet of the pump allowed controlling the temperature of the oil at the inlet of the PTC lines. A mass flow meter at the outlet of the pump was used to measure the oil mass flow rate. The temperatures at the inlet and at the outlet of the PTC were measured with temperature transmittance (TT) sensors. The direct normal irradiance (DNI) was measured with a pyrheliometer model CH1 by Kipp& Zonen [14]. A weather station installed nearby the solar field was used to measure the ambient temperature and the wind speed. The sensors signal outputs were acquired by a data acquisition system with a sampling time of 5 seconds and LabView was used for data visualization. During the experimental campaign on the PTTL facility, the EuroTrough collectors (ETC) line was tested. The ETC line was composed by 6 EuroTrough modules connected in series and 18 prototype receiver tubes from a Chinese manufacturer for a total length of 70.8 m and a net aperture area of 409.9 m^2.

3.2. Steady-state and dynamic experiments

In order to characterize the performance of the ETC test unit, xx steady-state points are collected for different operating conditions, by varying the pump speed velocity the temperature at the inlet of the ETC for a total of 5 days of testing. The system is run in stable conditions (RTD temperature variations below XX°C) for XX minutes and the steady-state point is recorded by averaging the measurements over a period of XX minutes. The acquired data are used to calibrate and to validate the model in steady-state. In order to characterize the dynamic performance of the ETC, the facility was run at different operating conditions by varying the pump speed velocity and the temperature at the inlet of the ETC. In Table 1, the working conditions ranges of the main variables and of the external ambient conditions during the experimental campaign are reported. The dynamic validation was based on three specific sets of experiments:

- **MFE** - Oil mass flow change experiment: a step change was imposed to the oil mass flow rate at the inlet of the

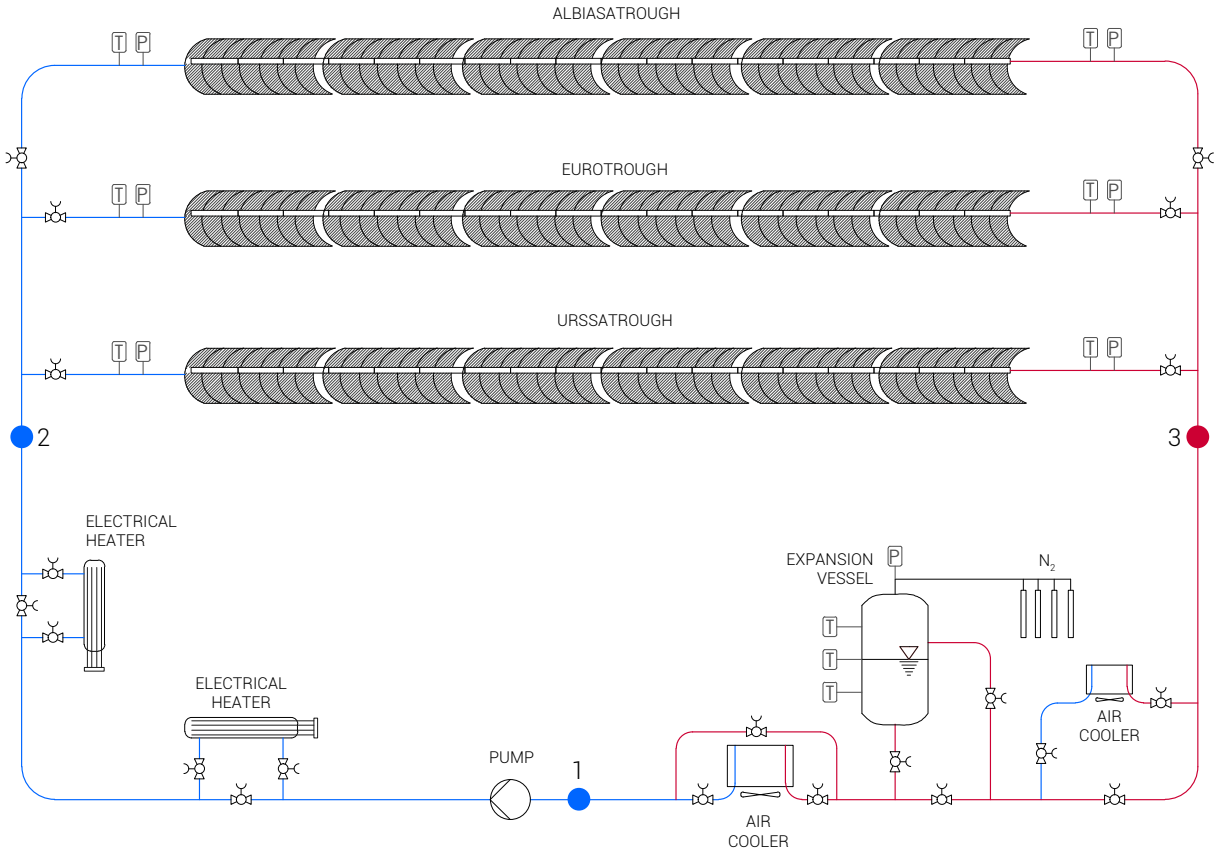

Figure 4: Process flow diagram of the PTTL facility with the relative sensors positions.

Table 1: Range of operation of the ETC main variable and of the external ambient condition during the experimental campaign.

Variable	$\dot{m}_{oil,su}$	$p_{SF,su}$	$T_{oil,su}$	$T_{oil,ex}$	DNI	T_{amb}	v_{wind}
Unit	[kg s^{-1}]	[bar]	[°C]	[°C]	[W m^{-2}]	[°C]	[m s^{-1}]
Min	1.55	12.96	150.05	170.21	593.95	26.23	0
Max	5.03	16.07	304.48	352.28	883.72	33.16	11.23

ETC by varying the pump speed velocity upwards or downwards starting from a steady-state condition.

- **TE** - Oil inlet temperature change experiment: the oil temperature at the inlet of the ETC was varied by shutting down the air cooler starting from a steady-state condition.

- **SBE** - Solar beam radiation change experiment: a step change to the solar beam radiations collected on the receiver was imposed downwards and upwards to the parabolic trough collectors by defocusing and focusing the parabolic trough collectors.

4. Simulation results and experimental validation

The steady-state and dynamic validation of the parabolic trough solar field (SF) dynamic model described in section 2 is presented in this section. The model is compared against experimental data acquired on the PTTL facility at the Plataforma Solar de Almería (PSA), Spain.

4.1. Initial conditions, model inputs and parameters

In order to compare the acquired dynamic experimental data with the modelling results a simulation framework was defined. A schematic representation of the system is shown in Figure 6. It comprised a mass flow source and a pressure sink connected to the fluid connectors of the SF model. The exogenous inputs (EI) imposed to the SF model

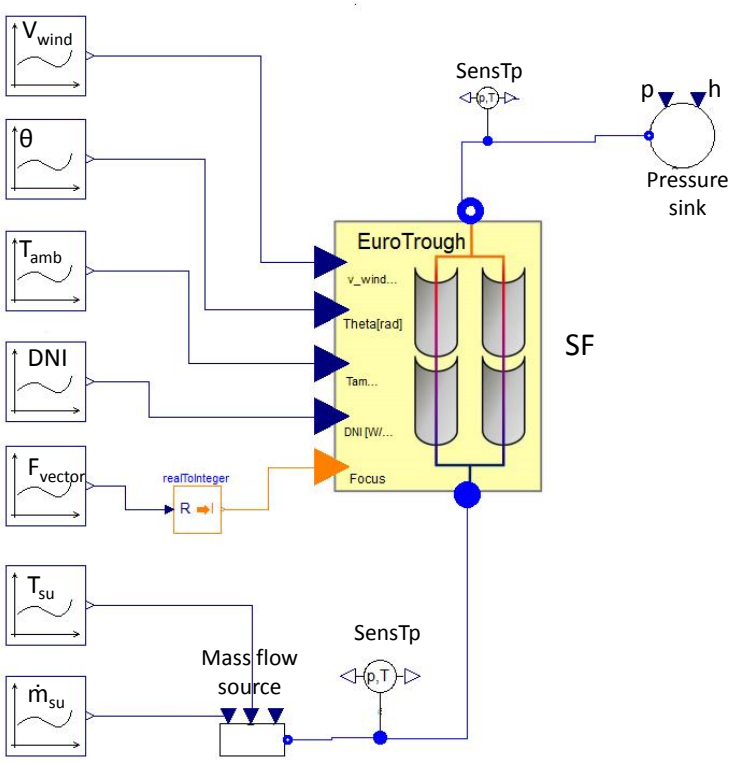

Figure 5: Modelica model of the Eurotrough collector line installed in the PTTL facility from the Dymola graphical user interface (GUI).

and the relative unit are listed in Table 2. The SF model was parametrized based on the data-sheets of the EuroTrough collector and the receiver tubes. The incidence angle modifier (IAM), required for the optical efficiency calculation, was computed with an empirical equation as:

$$IAM = 1 - \frac{a_{\mathrm{I}} \cdot \Theta_{\mathrm{incid}} + a_{\mathrm{II}} \cdot \Theta_{\mathrm{incid}}^2}{\cos \Theta_{\mathrm{incid}}} \tag{6}$$

where Θ_{incid} is the incidence angle of solar radiation and $a_{\mathrm{I}} - a_{\mathrm{II}}$ are two empirical parameters derived through an experimental campaign as described in [15] following the methodology presented in [16]. In order to consider unaccounted optical effects during testing, e.g., dirt on the parabolic mirrors and tube receivers, the parameter ϵ_{un} was

Table 2: List of exogenous inputs (EI) imposed to the SF model.v_{wind}: wind speed, Θ_{incid}: solar radiation incidence angle, T_{amb}: ambient temperature, DNI: direct normal irradiance, F_{vector}: vector for defocusing action, $\dot{m}_{oil,su}$: oil mass flow at SF inlet, $T_{oil,su}$: oil temperature at SF inlet, p_{ex}: oil pressure at SF outlet

EI	v_{wind}	Θ_{incid}	T_{amb}	DNI	F_{vector}	$\dot{m}_{\text{oil,su}}$	$T_{\text{oil,su}}$	p_{ex}
Unit	[m s^{-1}]	[Rad]	[°C]	[W m^{-2}]	[-]	[kg s^{-1}]	[°C]	[bar]

Table 3: Values of the parameters for the SF Modelica model

Parameter	Units	Value
General parameters		
N - Number of discretized cells	[-]	20
L - PTC length	[m]	70.8
A_p - Parabola aperture	[m]	5.76
Optical properties		
ρ_{cl} - Mirror reflectivity	[-]	0.9388
τ_{gl} - Glass transmissivity	[-]	0.92
α_{gl} - Glass absorptivity	[-]	0.02
ϵ_{gl} - Glass emissivity	[-]	0.86
α_{tu} - Tube Absorptivity	[-]	0.7919
a_{I} - IAM coefficient I	[-]	$4.11e^{-3}$
a_{II} - IAM coefficient II	[-]	$5.513e^{-5}$
ϵ_{un} - Unaccounted	[-]	0.9437
Glass envelope geometries		
D_{gl} - External glass diameter	[m]	0.12
t_{gl} - Glass thickness	[m]	0.0025
Receiver tube geometries		
D_{tu} - External glass diameter	[m]	0.07
t_{tu} - Glass thickness	[m]	0.002
Vacuum properties		
p_{vacuum} - Vacuum pressure	[bar]	$1.333e^{-7}$
Γ - Ratio of specific heats for the annulus gas	[-]	1.39
Δ_{mol} - Molecular diameter for the annulus gas	[m]	$3.53e^{-10}$
k_{std} - Thermal conductivity at standard pressure and temperature	[W $m^{-1}K^{-1}$]	0.02551

included in the calculation of the optical efficiency. Its value was obtained through a least square optimization routine aimed at minimizing the error between the simulated SF outlet temperature and the measured one over a three minutes interval of the initial steady-state condition characterizing the first day of testing (see Figure 9). In Table 3 the values assigned to the parameters of the SF model are reported.

The *GlassUD* and *TubeUD* options were set to false such that the density, specific heat capacity and thermal conductivity of the glass and the metal tube were computed as dependent on the glass and tube temperatures respectively. The heat transfer coefficient was computed based on the Gnielinski single phase correlation [17]. The thermal oil, Syltherm 800, flowing through the tube receivers was modelled as an incompressible fluid using the *TableBased* framework of the Modelica Standard library. As a consequence no mass accumulation was considered in the receiver tubes.

4.2. Results: Steady-state validation

The SF model is compared against the 24 collected steady-state experimental points. The data are acquired at different temperature levels at the inlet of the collectors, by varying the pump rotational speed and the thermal input of the heaters and air coolers . In Figure 3, the model prediction for the temperature at the outlet of the collectors are plotted versus the experimental values.

The developed model is able to reproduce the measured data points with a good agreement. The temperature at the outlet of the collectors is characterized by an accuracy within 3°C.

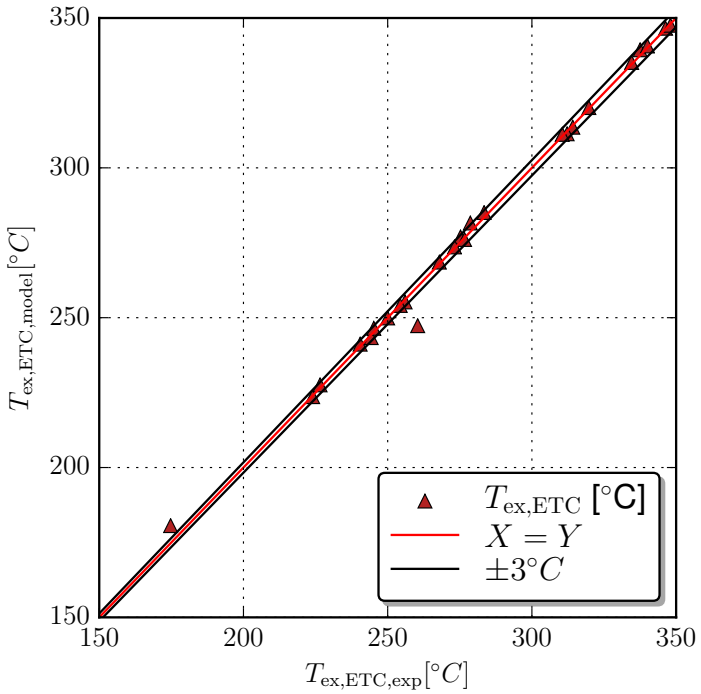

Figure 6: Parity plot for the ETC outlet temperature.

4.3. Results:Dynamic validation

The SF Modelica model was run on Dymola2015. The Differential Algebraic System Solver (DASSL) [18] was selected as numerical solver, setting the relative tolerance to 10^{-4}. In order to increase the model robustness and decrease the computational time, the measured variables imposed as exogenous inputs to the SF model (see Table 2) are approximated by a spline function in the Modelica/Dymola simulation environment.

In Figure 7, the simulated ETC outlet temperature is plotted versus time and compared against the measured data for each of the three performed dynamic experiments. On the left abscissa the measured ETC inlet and outlet temperatures and the simulated ETC outlet temperature are plotted versus time. On the right abscissa the DNI and oil mass flow rate normalized with respect to the maximum value reached during the day are reported. For all the plots it is possible to see how the DNI was characterized by variation smaller than 2%. In Figure 7a the results for the MFE experiments and simulation results are reported. Starting from a steady-state condition two consecutive steps of the same magnitude upwards and downwards were imposed to the pump rotational speed at t=450 seconds and t=1430 seconds respectively. As the rotational speed increased at t=450 seconds, the velocity and pressure of the fluid in the high pressure line increased. This resulted in an oil mass flow rate, $\dot{m}_{\mathrm{oil,su}}$, increment of about 40% in around 60 seconds. The increase in oil mass flow rate caused a drop in the temperature at the outlet of the ETC, $T_{\mathrm{oil,ex}}$. The $T_{\mathrm{oil,ex}}$ drop was registered at around t=500 seconds, 50 seconds after the oil mass flow rate started changing. This

was due to the time required by the oil mass flow rate to reach the outlet of the 70.8 m long receiver tubes. During the experiments the ETC inlet temperature, $T_{\text{oil,su}}$, was maintained constant by manually manipulating the air cooler and electrical heaters power. When the oil mass flow rate was changed upwards, as $T_{\text{oil,su}}$ was expected to decrease the air cooler power was decreased and the electrical heaters power was increased manually, causing a small bump within 2 K in the temperature as it is shown in Figure 7a. The same phenomena in the opposite direction took place when the pump speed was decreased. The ETC outlet temperature presented a symmetrical trend for the upwards and downwards oil mass flow rate change. The SF model was able to well predict the experimental trend both for the upward and downward steps and was characterized by a time constant slightly smaller than the real system.

In Figure 7b the TE experiments and simulation results are reported. Starting from a steady-state condition the air-cooler was turned off at t=900 seconds. This resulted in an increase of $T_{\text{oil,su}}$ and a consequently growth of $T_{\text{oil,ex}}$ delayed by around 100 seconds due to the time required by the oil mass flow to travel through the tube receiver. The shut-down of the oil-cooler did not allow to impose a step to $T_{\text{oil,su}}$ which increased with a slow first order trend. The large time constant characterizing $T_{\text{oil,su}}$ defined the change of the outlet ETC temperature. The SF model was able to correctly predict the experimental results including the delay characterizing the $T_{\text{oil,ex}}$ change.

Finally in Figure 7c the SBE experiments and simulation results are shown. Starting from a steady-state condition the ETCs were defocused at t=360 seconds, such that no solar radiation was reflected to the receiver tubes. This caused a sudden decrease of $T_{\text{oil,ex}}$ which reached the $T_{\text{oil,su}}$ value in about 200 seconds. The ETCs were focused again at t=650 bringing $T_{\text{oil,ex}}$ back to its initial value. During the experiment the oil mass flow rate and $T_{\text{oil,su}}$ were kept constant. The latter was maintained at its initial value by manually manipulating the power of the two electrical heaters installed after the pump. This resulted in a small bump of less then 4 K after the collectors were focused at t=700 seconds. The $T_{\text{oil,ex}}$ was characterized by a symmetrical behaviour during the focusing-defocusing experiments, as the thermal energy losses were relatively small. The SF model was able to replicate the trend and presented a slightly smaller time constant than the real system.

Overall it can be concluded that the SF Modelica model was capable of predicting the physical phenomena characterizing the real system behaviour during the three performed experiments and can be considered validated.

In Figure 9 the simulation and experimental results for all of the five days of the experimental campaign are reported. In the first Figure, *Day I*, the three minutes time over which the ϵ_{un} parameter was optimized are highlighted by two vertical black dotted lines.

5. Discussion

This work aims at proposing tools to analyse the unsteady operations of parabolic through collectorss, with a special attention for the following characteristics:

- Satisfactory accuracy for engineering scopes
- Low computational time

The model of the parabolic through is based on the finite volume method, characterized by a trade-off between model accuracy and computational time: increasing the number of CVs leads to better accuracy but negatively affects the computational effort.

In order to investigate the effect of the level of discretization on the performance of the SF model when compared to the experimental results a parametric analysis was performed. The SF model, discretized with a number of control volumes (CVs) varying from 1 to 50, was simulated to replicate the experimental data of Day *IV* (see Figure 9). The results are displayed in Figure 10a where the simulated SF outlet temperature for the different levels of discretization is plotted versus time and compared against the measured experimental data on the left abscissa. On the right abscissa the nominal DNI and oil mass flow rate are plotted. Overall as the level of discretization increased the SF outlet temperature got closer to the measurements data. From 10 to 50 CVs the improvement in model accuracy was negligible. On the other hand the 5 CVs and 1 CVs SF model presented a slower time constant compared to the real system and were not able to properly predict the different undershoot and overshoot characterizing the measured outlet ETC temperature when the boundary conditions where changed, e.g., step change in the mass flow or defocusing-focusing.

In Figure 10b the percentage computational effort (PCE) defined in equation 7 as the ratio of the computational time ($\text{Time}_{\text{Comp}}$) with respect to the simulated real time ($\text{Time}_{\text{Real}}$), is plotted for each simulation result. All the simulation results were characterized by a much shorter time compared to the real simulated time. This is related to the remarkably simple simulation framework on which the modelling results were based on (see section 4.1).

$$\text{PCE} = \frac{\text{Time}_{\text{Comp}}}{\text{Time}_{\text{Real}}} \cdot 100 \tag{7}$$

The computational time increased exponentially with the increase of number of CVs with the 1 and 5 CVs SF models being one order of magnitude faster than the higher discretized model.

In order to assess the discrepancy between the different CVs discretization levels, the total energy absorbed by the thermal oil in the ETC collectors, E_{oil}, was computed as the integral of the thermal power over the simulated time, around 4 hours, and compared with respect to the 50 CVs model which was taken as a reference. The percentage relative error $\bar{\epsilon}$ for each SF model was computed as:

$$\bar{\varepsilon}(k) = 100 \cdot \frac{|E_{\text{oil,50CVs}} - E_{\text{oil,k}}|}{E_{\text{oil,50CVs}}} \quad k \in [1, 5, 10, 20]. \tag{8}$$

Table 4: Total energy percentage relative error for the different levels of discretization of the SF model.

Model	$\bar{\varepsilon}$ [%]
SF CVs 1	0.5
SF CVs 5	0.18
SF CVs 10	0.08
SF CVs 20	0.03

The results are reported in Table 4. As it possible to see, the overall percentage relative error on the total energy absorbed by the fluid over 4 hours of simulation with respect to the 50 CVs SF reference model was negligible for all the tested levels of discretization.

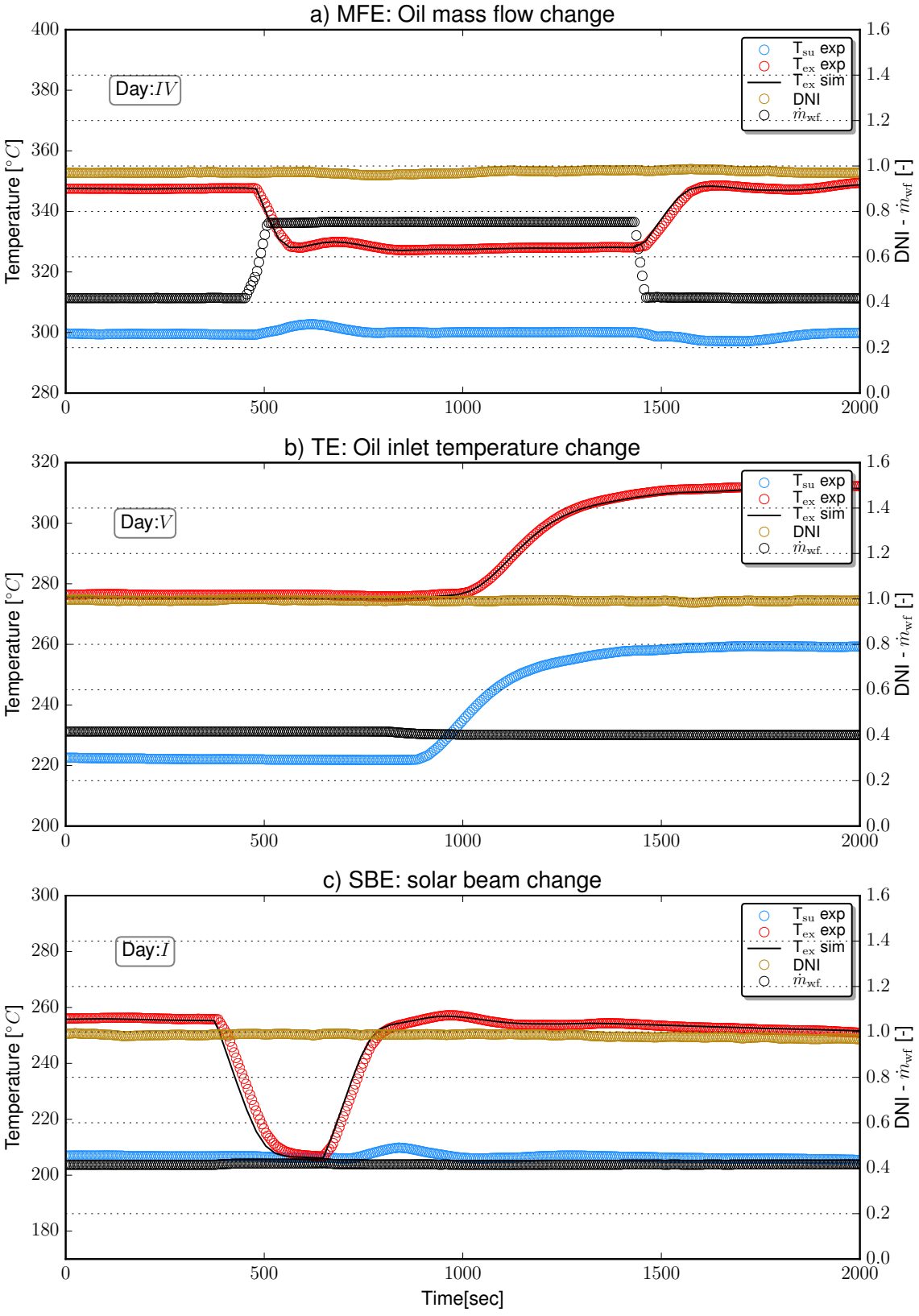

Figure 7: Simulation and experimental results plotted versus time for: a) MFE - Mass flow change experiment b) TE - inlet ETC temperature change experiment c) SBE - solar beam radiation change experiment. The measured inlet and outlet ETC temperatures and the outlet SF model temperature are plotted on the left abscissa. The normalized DNI and oil mass flow rate values are plotted on the right abscissa.

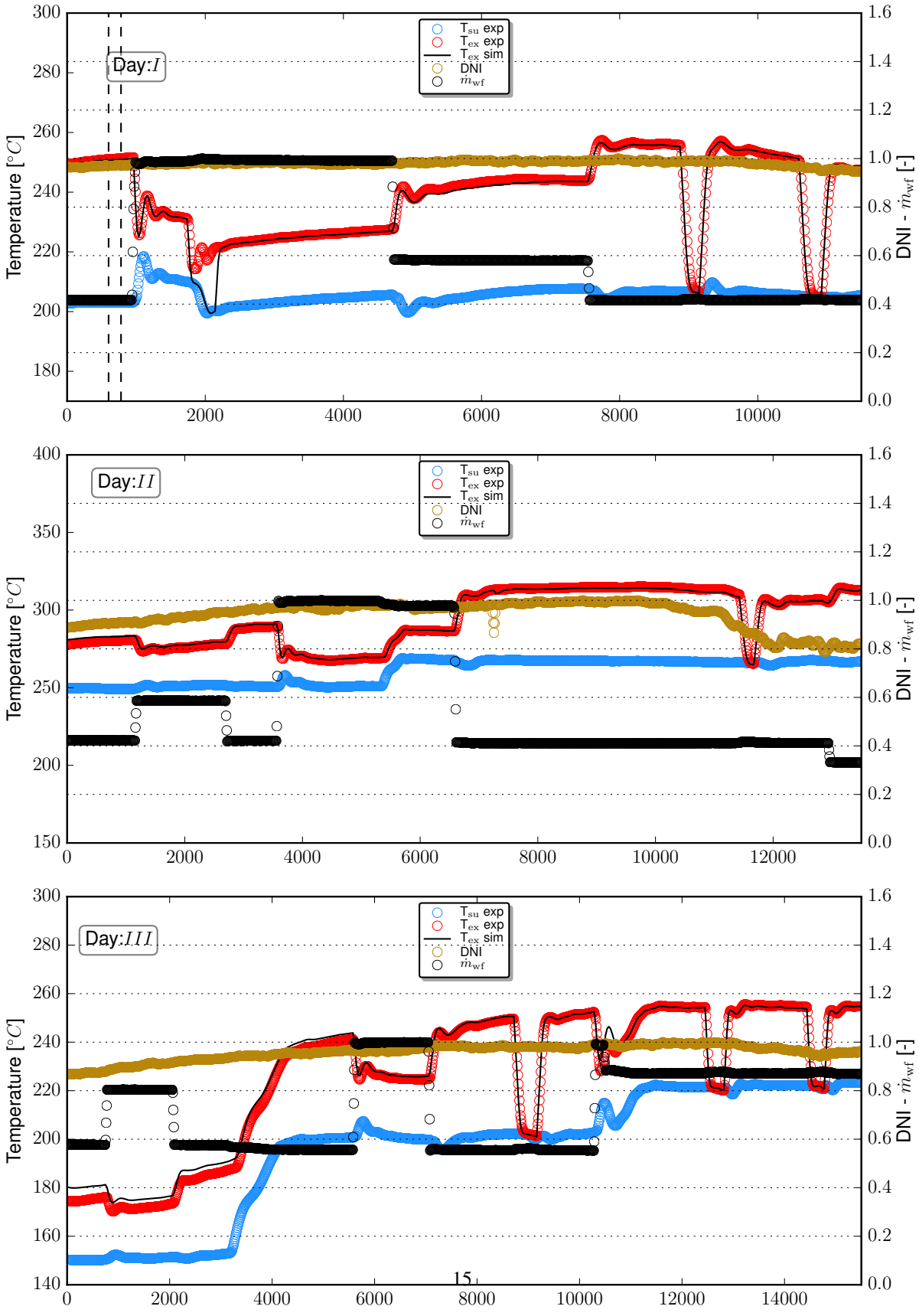

Figure 8: Simulation versus experimental results for the first three days of the experimental campaign plotted versus time.

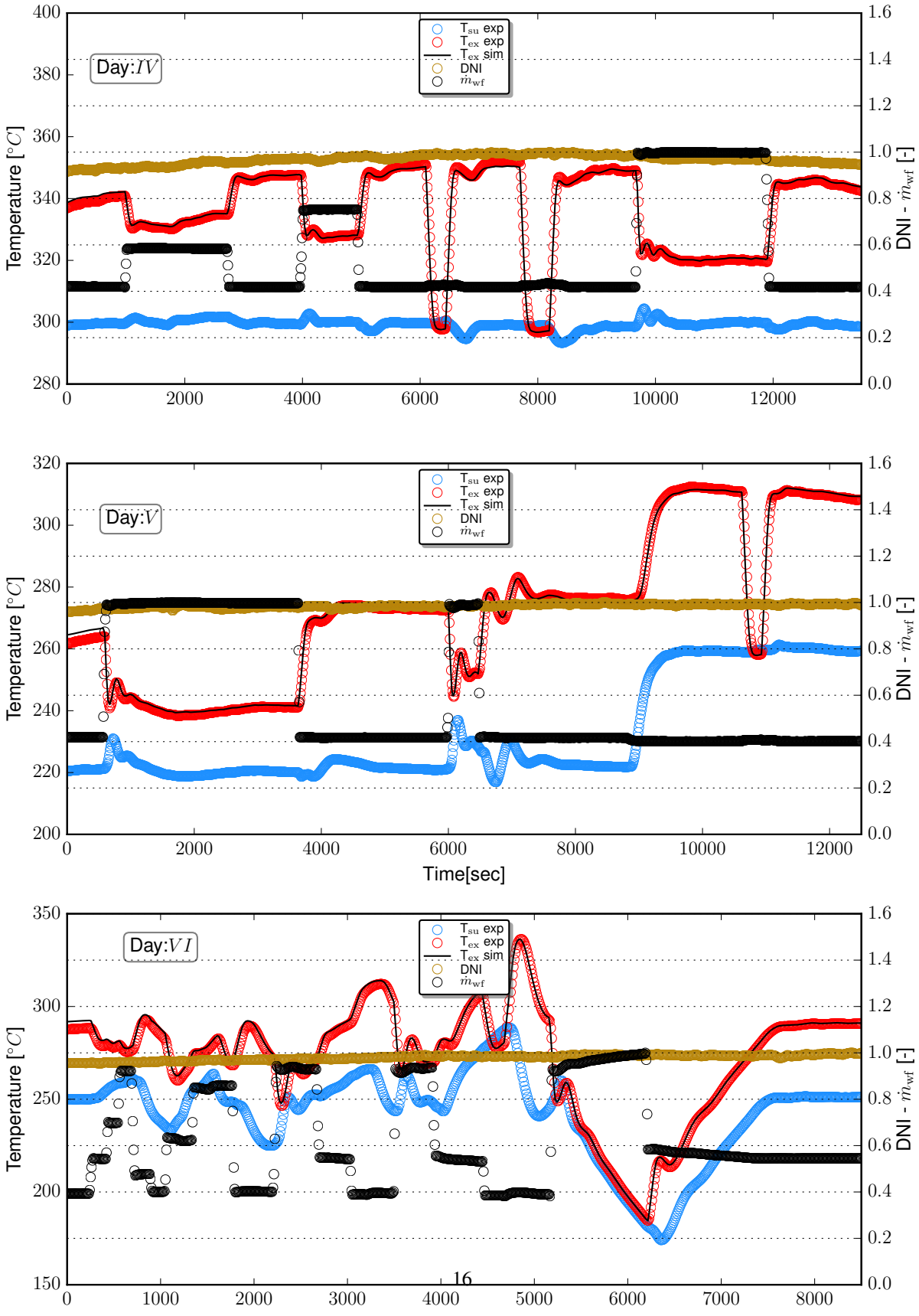

Figure 9: Simulation versus experimental results for the second three days of the experimental campaign plotted versus time.

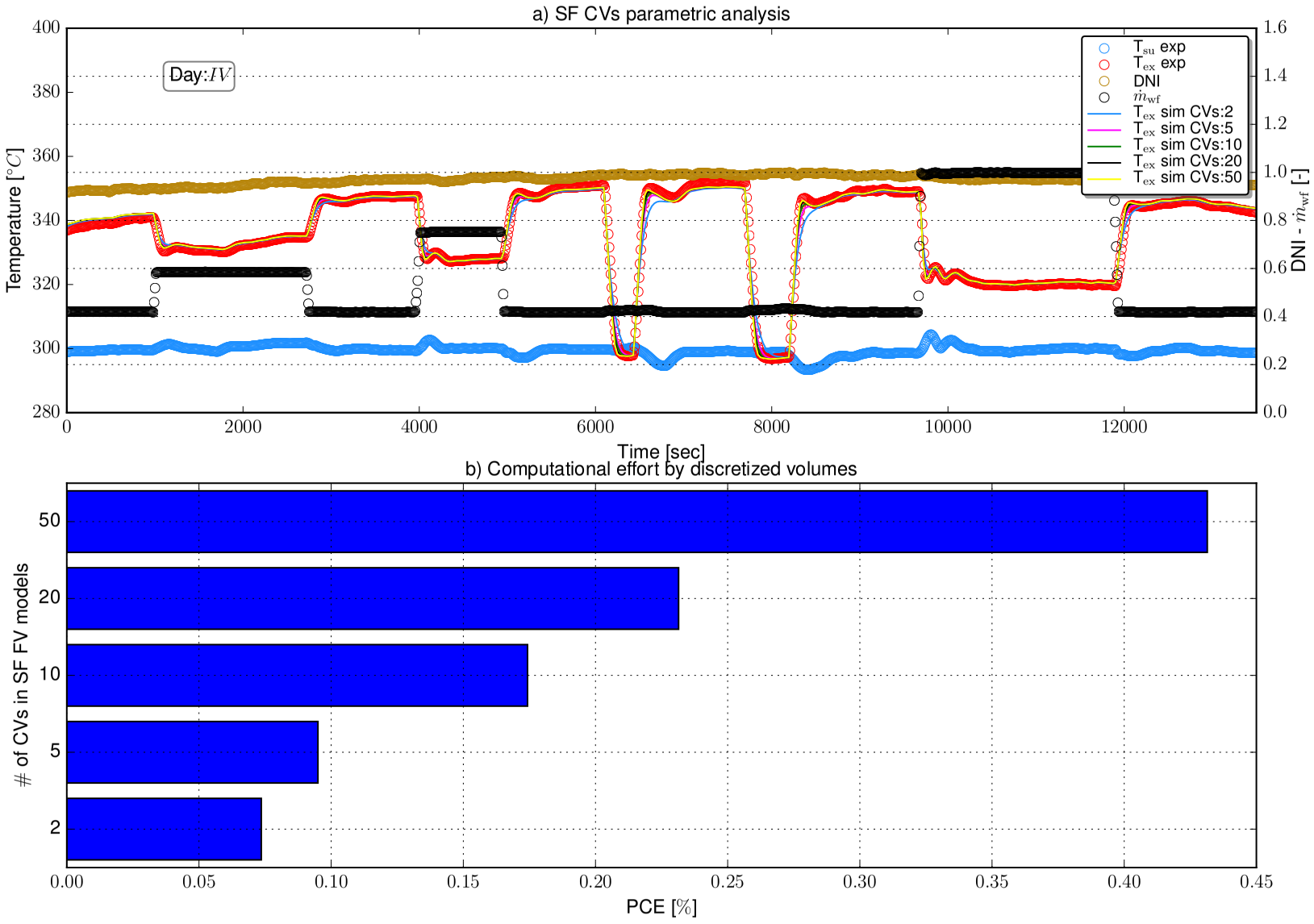

Figure 10: Simulation results versus the experimental results for each full day of the experimental campaign. PCE: percentage computational effort.

6. Conclusions

The parabolic trough ThermoCycle Modelica model was compared against experimental data acquired on the PTTL facility at the Plataforma Solar de Almería (PSA), Spain. Dynamic experiments were performed by varying the oil mass flow rate (MFE), the oil inlet temperature (TE) and the direct beam solar radiation (SBE) for different operating conditions.

- The simulation results obtained for the oil mass flow change experiment(MFE), the oil inlet temperature change experiment (TE) and the solar incidence beam radiation experiment (SBE) showed a good overlap with the experimental results. The developed solar field model structure proves to be effective to predict the dynamic of a real solar field.

- A minimum discretization level of 20 CVs was found to be a good compromise between model accuracy and simulation speed if the ETC outlet temperature had to be precisely predicted, e.g., the SF model is used as a reference to develop and test model based control strategies.

- In light of the obtained results a lumped SF model is recommended if the performance of the ETC collectors are analysed on a daily or longer time frame. This approach allows to significantly decrease the computational time while maintaining a satisfying level of accuracy.

It was proven that the modelling approaches adopted led to satisfactory results for the simulation of parabolic trough collector systems.
The proposed solar collector model together with the test cases is released as open-source and is available in the latest version of the ThermoCycle library.

7. Acknowledgements

The results presented in this paper have been obtained within the frame of the SFERA II project.

References

[1] Casati E, Desideri A, Casella F, Colonna P. Preliminary Assessment of a Novel Small CSP Plant Based on Linear Collectors , ORC and Direct Thermal Storage. SolarPaces Conference 2012;.

[2] Prabhu E. Solar Trough Organic Rankine Electricity System (STORES) Stage 1 : Power Plant Optimization and Economics. Tech. Rep. March; 2006. doi:NREL/SR-550-39433.

[3] Verneau A. L'emploi des fluides organiques dans les turbines solaires. Entropie 1978;:9 – 18.

[4] Angelino G, Gaia M, Macchi E. A review of italian activity in the field of organic Rankine cycles. Verein Deutscher Ingenieure Berichte 539 1984;:465–82.

[5] Ray A. Nonlinear dynamic model of a solar steam generator. Solar Energy 1981;26(4):297 – 306.

[6] T. H, M. E, W.D. S. Simulation of transient two-phase flow in parabolic trough collectors using Modelica. In: Proceedings of the 4th International Modelica Conference. 2005,.

[7] Bonilla J, Dormido S, Cellier FE. Switching moving boundary models for two-phase flow evaporators and condensers. Communications in Nonlinear Science and Numerical Simulation 2015;20(3):743–68.

[8] Elmqvist H. A Structured Model Language for Large Continous Systems. Ph.D. thesis; Lund Institute of Technology; 1978.

[9] Quoilin S, Desideri A, Wronski J, Bell IH, Lemort V. ThermoCycle: A Modelica library for the simulation of thermodynamic systems. In: Proceedings of the 10^{th} International Modelica Conference. 2014,.

[10] Bell I, Wronski J, Quoilin S, Lemort V. Pure- and Pseudo-Pure Fluid Thermophysical Property Evaluation and the Open-Source Thermophysical Property Library CoolProp. Industrial & Engineering Chemistry Research 2014;53:2498–508. doi:10.1021/ie4033999.

[11] Forristall R. Heat Transfer Analysis and Modeling of a Parabolic Trough Solar Receiver Implemented in Engineering Equation Solver. Tech. Rep. October; National Renewable Energy Laboratory; 2003.

[12] Desideri A. Dynamic modeling of organic rankine cycle power systems. 2016.

[13] Dow Oil and Gas . Syltherm 800 Heat Transfer Fluid. Tech. Rep.; DOW; 1997.

[14] Kipp , Zonen . CH1 NIO (normal incidence pyrhelimeter) manual; 1997. URL: `http:// www.kippzonen.com`.

[15] Sallaberry F, Valenzuela L, de Jalón AG, Leon J, Bernad ID. Towards standardization of in-site parabolic trough collector testing in solar thermal power plants. AIP Conference Proceedings 2016;1734:130019–1. doi:10.1063/1.4949229.

[16] Valenzuela L, López-Martín R, Zarza E. Optical and thermal performance of large-size parabolic-trough solar collectors from outdoor experiments: A test method and a case study. Energy 2014;70:456–64. doi:10.1016/j.energy.2014.04.016.

[17] Gnielinski V. Heat Transfer in Pipe Flow. VDI Heat Atlas 2010;:691–700doi:10.1007/978 – 3 – 540 – 77877 – $6_3$4.

[18] Petzold LR. A description of DASSL: a differential-algebraic system solver. Scientific computing 1983;94550:65–8.